

# Failure Mechanism of Reinforced Concrete Structural Walls with and without confinement



**A. Benavent-Climent, D. Escolano-Margarit,**

*University of Granada, Granada, Spain*

**A. Klenke & S. Pujol**

*Purdue University, West Lafayette, Indiana, US*

## **SUMMARY: (10 pt)**

This paper presents the results of cyclic loading tests on two large-scale reinforced concrete structural walls that were conducted at Purdue University. One of the walls had confinement reinforcement meeting ACI-318-11 requirements while the other wall did not have any confinement reinforcement. The walls were tested as part of a larger study aimed at identifying parameters affecting failure modes observed to limit the drift capacity of structural walls in Chile during the Maule Earthquake of 2010. These failure modes include out-of-plane buckling (of the wall rather than individual reinforcing bars), compression failure, and bond failure. This paper discusses the effects of confinement on failure mode. Distributions of unit strain and curvature obtained with a dense array of non-contact coordinate-tracking targets are also presented.

*Keywords: Structural Wall, Cyclic Test, Plastic Hinge.*

## **1. INTRODUCTION**

Structural walls have been commonly used during the past decades as a lateral load resisting system against earthquake. The field observations during the Maule Earthquake of 2010 in Chile have shown that due their high bending stiffness structural walls reduced story drifts concentrating the structural damage in the lower levels. However It is necessary a flexural mode of failure in the plastic hinge regions to avoid a brittle shear failure and to ensure a desired ductile behaviour. Several authors studied and proposed the requirements to ensure that the lateral shear strength is higher than the flexural strength. Krollicki, J. et al (2011) proposed a shear strength model based on previous experimental research. Hidalgo et al. (2002) studied the behaviour of 26 full-scale shear walls characterized by shear mode of failure. Pilakoutas & Elnashai (1995) tested nine 1:2.5 scale isolated shear walls under cyclic loading in order to determine the ductility and the energy absorption potential of RC walls. Another important factor to take into account in the seismic design of RC structural walls is the estimation of the inelastic flexural displacement of the structural walls by assuming a concentration of inelastic curvatures at the wall base which are referred as plastic hinges. For the sake of simplicity, the inelastic curvatures,  $\phi_i$ , in a plastic hinge are commonly assumed constant over the length of the plastic hinge,  $l_p$ . Once the plastic hinge length is determined the inelastic wall displacement,  $\Delta_i$ , can be easily obtained by integrating the curvatures over the wall height. An accurate assessment of the plastic hinge length is essential to obtain reliable estimations of the inelastic displacements. Researchers during the last decades have proposed several expressions in order to estimate the plastic hinge length in RC columns and beams (Bae, S. & Bayrak, O. (2008); Priestly, M. J. N., & Park, R. (1987); Sheikh, S. A., & Khoury, S. S. (1993)). However there is a lack of information in the case of structural walls. Dazio, A. et al (2009) suggested several strain limits for plastic hinge analysis based on the curvature measured at the base of six shear walls during a cyclic loading test. Bohl, A., & Perry, A. (2011) proposed a plastic hinge length based on the results of non-linear finite element analyses.

This paper presents the results from two large-scale reinforced concrete structural wall tests that were conducted at Purdue University. One of the specimens differs from the other in the inclusion of confinement reinforcement at the boundary elements. The main goal of this paper is to discuss the effects of confinement on failure mode. The experimental results of unit curvature and unit strain distribution presented in this paper also contribute to a better understanding of the plastic hinge length in structural walls.

## 2. EXPERIMENTAL INVESTIGATION

Two large-scale reinforced concrete structural walls were tested under quasi-static cyclic loading conducted at Purdue University. One of the specimens called W-MC-C herein after had confinement reinforcement while the other called W-MC-N herein after did not have any confinement reinforcement.

### 2.1. Structural wall design

Specimen W-MC-C shown in Figure 1 was designed to meet ACI-318-11 ACI Committee 318 (2011) confinement reinforcement requirements. The longitudinal reinforcement was comprised of 4 #8 bars for the confinement element and 3 #4 bars in the wall. The confinement reinforcement is comprised of #2 stirrups around the boundary elements spaced at 2.5 in. c. to c. up to 5 ft.. Also there are #3 ties that are spaced at 5 in. c. to c. spacing in the wall. Specimen W-MC-N shown in Figure 1 has the same layout except for the confinement reinforcement. Both specimens had mechanical couplers at the base of the wall which torque the longitudinal bars from the wall and the footing together. The yield stress,  $f_y$ , and ultimate stress,  $f_u$ , of the reinforcement as well as the compressive stress,  $f_{ck}$ , tensile stress,  $f_{ct}$ , and Module of elasticity,  $E_c$ , of the concrete can be found in Table 1.

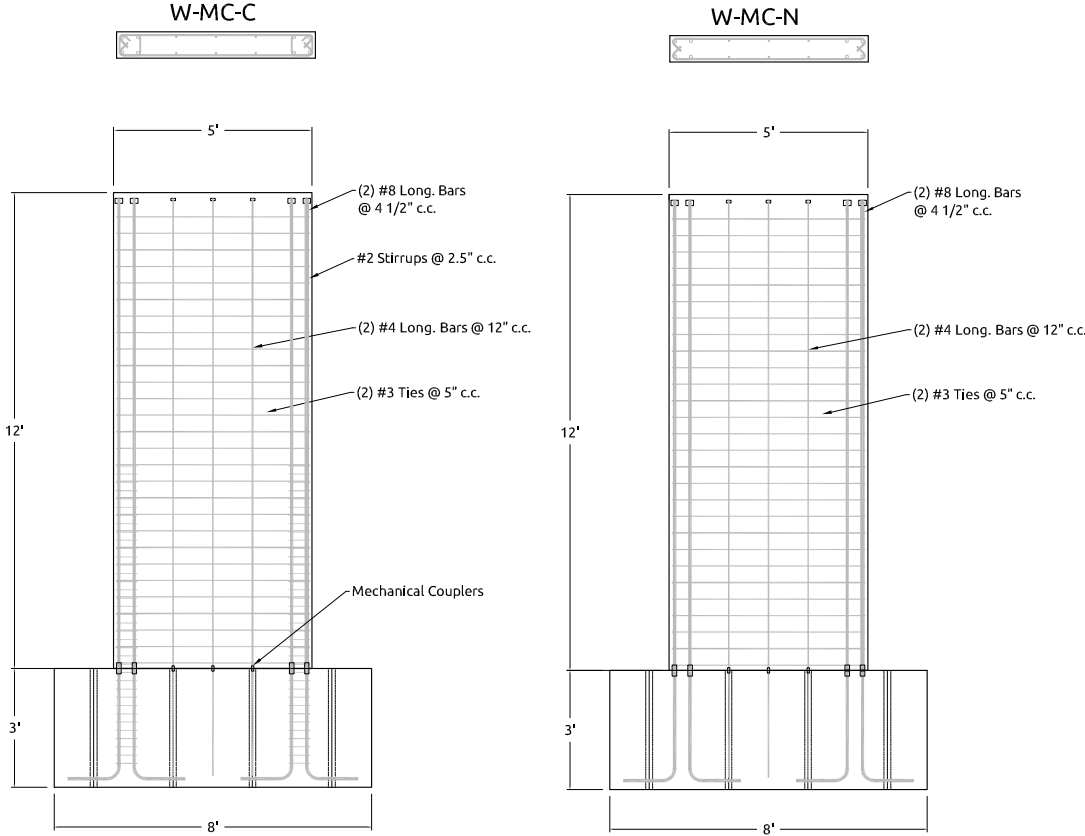


Figure 1: Geometry and reinforcement

Table 1: Mechanical properties of materials

Steel			Concrete						
Bar Size #	$f_y$ (ksi)	$f_{su}$ (ksi)		WMCC			WMCN		
				$f_{ck}$ (psi)	$f_{ct}$ (psi)	$E_c$ (ksi)	$f_{ck}$ (psi)	$f_{ct}$ (psi)	$E_c$ (ksi)
2	69	80	Footing 1	5105	453	3645	5059	392	3645
3	70	98	Footing 2	4606	473	3224	4570	395	3604
4	62	90	Lift 1	4455	468	3637	4467	406	3569
8	67	94	Lift 2	5033	427	3873	5130	423	3740
9	63	98	Lift 3	4790	421	4010	5068	445	3990

### 3. SET-UP, INSTRUMENTATION AND LOADING HISTORY

The structural walls were fixed to the strong floor by 8 large diameter post-tensioning bars. An auxiliary loading structure was connected on top of the wall to two symmetrical hydraulic actuators with hinges at both ends. The force capacity of the actuators was 110 kips and a displacement capacity of 30 inch each. The axial load was applied by two steel beams, placed on the wall head perpendicular to the loading direction. The load was applied by four post-tensioning bars connected to both ends of the axial load beams and directly to the strong floor. The bars were post-tensioned by 4 jacks situated on the live anchor at the top of the walls. Two load cells named LC1 and LC2 in Figure were placed between the jack and the axial load system to control and to keep the axial load constant throughout the tests. Two auxiliary steel beams were placed on either side of the wall parallel to the loading direction to prevent the out of plane failure of the walls. Figure shows the experimental set up during the tests.

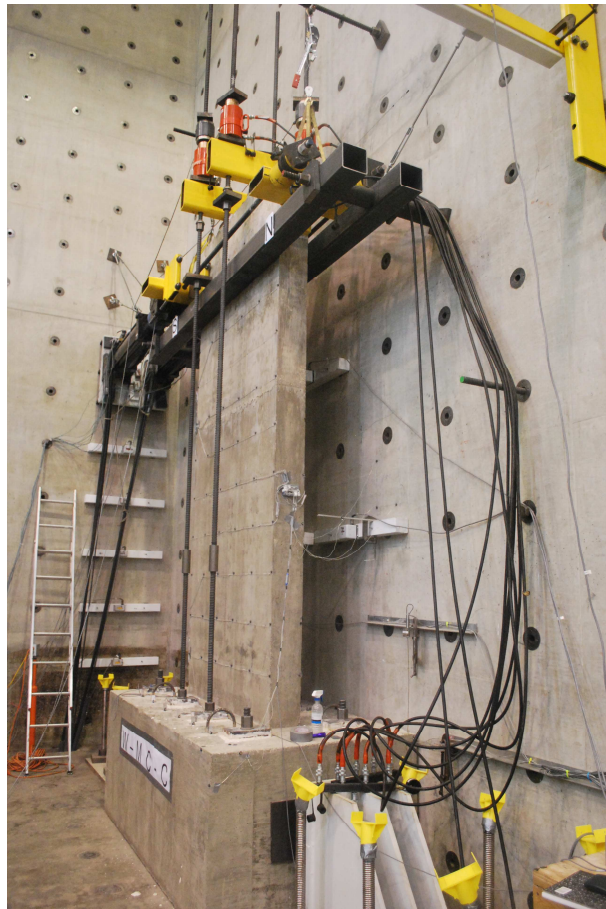


Figure 3: Experimental Set-up.

### 3.1. Instrumentation

During each cycle the response of the walls, load and displacements, was measured with the following sensors: (i) Load cells LC1 and LC2 measured the applied load. (ii) Load cells LC3 and LC4 measured the axial load. (iii) Displacement encoders, ENC 1 to 8 and 12, measured the displacements in the direction of the loading while displacement encoders ENC 9 to 11 measured the out of plane displacements. (iv) The coordinates of 62 non contact coordinate-tracking targets forming a 1 by 1 ft grid were measured at the maximum drift instant of each cycle. The notation and position of instruments are shown in Figure .

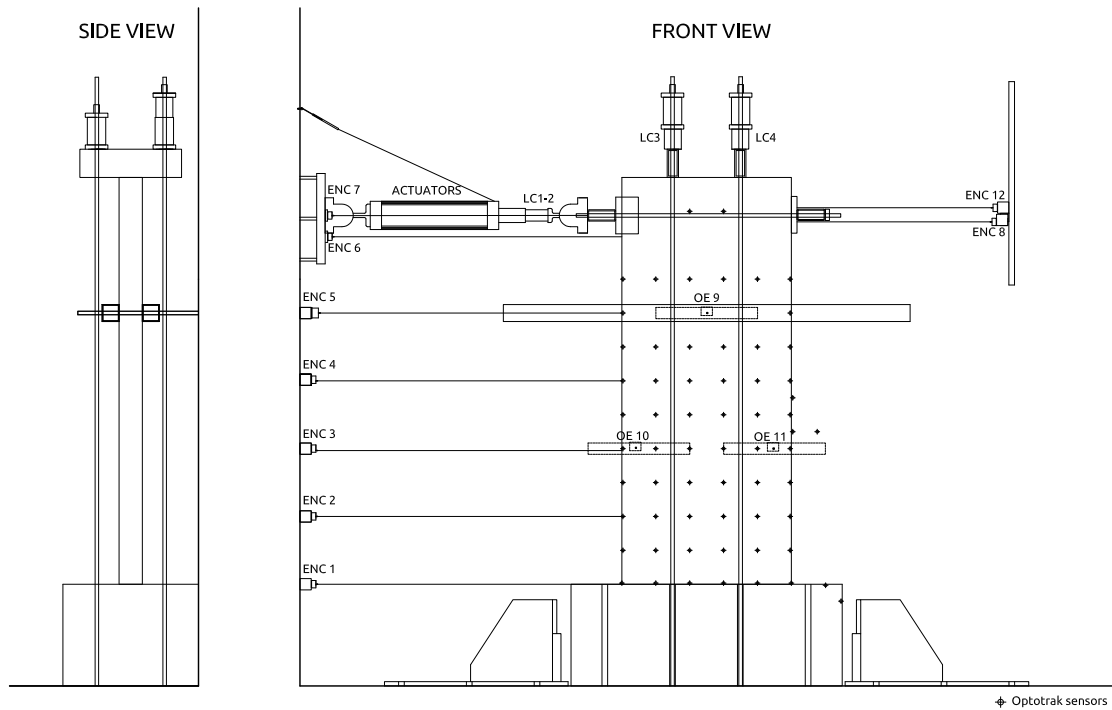


Figure 4: Instrumentation

### 3.2. Loading history

Initially the axial load was applied with a value of  $0.1 f_c' A_g$ . The axial load was kept approximately constant during the tests. The imposed horizontal displacement history at the walls head is shown in

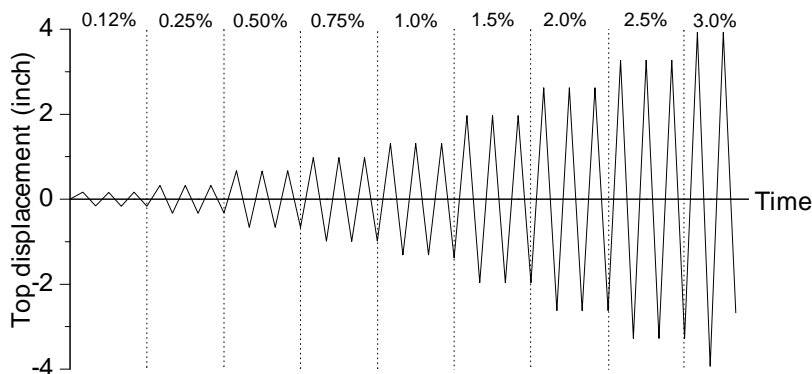


Figure . As can be observed the cyclic displacement consisted in applying three cycles at each drift level. The drift levels considered were 0.12, 0.25, 0.5, 0.75, 1.0, 1.50, 2, 2.5 and 3.0% expressed as percentage of the wall height.

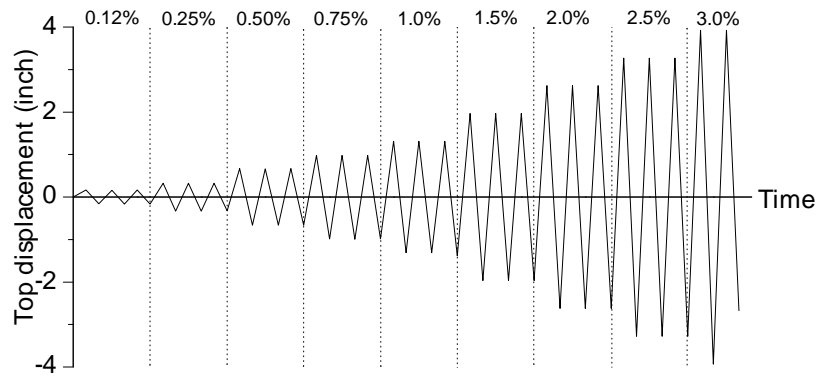


Figure 5: Loading history

## 4. TESTS RESULTS.

### 4.1. Specimen W-MC-C

First cracking was observed in cycle #1 at a load of 46 kips and 0.17 inch of displacement. First yield occurred in cycle #10 at a load of 137 kips and 0.98 inch of displacement. Compression vertical cracks and spalling at the base of the boundary elements was observed from cycle #11 in advanced. The maximum strength of 163 kips was reached at cycle #25 at 3.93 inch of displacement. The wall collapsed in cycle #26 due to the buckling of the boundary element reinforcement. Figure a show the load versus top displacement hysteresis curve. As can be seen the behaviour of the wall was clearly controlled by a flexural mode of failure. Figure show photographs of the crack patterns at the base for several limit states. The maximum crack width measured during the tests was 0.005, 0.03 and 0.15 inch for the flexural cracking, first yield and ultimate capacity limit states.

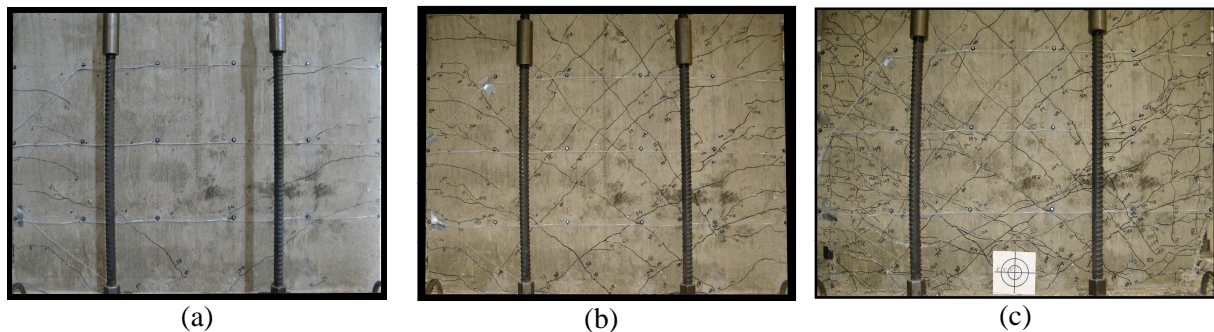


Figure 6: Crack patterns for limit states: (a) Flexural cracking. (b) First yield (c) Ultimate capacity

### 4.2. Specimen W-MC-N

First cracking was observed in cycle #1 at a load of 42 kips and 0.16 inch of displacement. Compression vertical cracks and spalling at the base of the boundary elements was observed from cycle #9 in advanced. First yield occurred in cycle #10 at a load of 137 kips and 0.98 inch of displacement. The maximum strength of 155 kips was reached at cycle #14 at 2.62 inch of displacement. The wall collapsed in cycle #19 due to the buckling of the reinforcement. Figure b show the load versus top displacement hysteresis curve. As can be seen the behaviour of the wall was clearly controlled by a flexural mode of failure. Figure show photographs of the crack patterns at the base for several limit states. The maximum crack width measured during the tests was 0.005, 0.025 and 0.15 inch for the flexural cracking, first yield and ultimate capacity limit states.

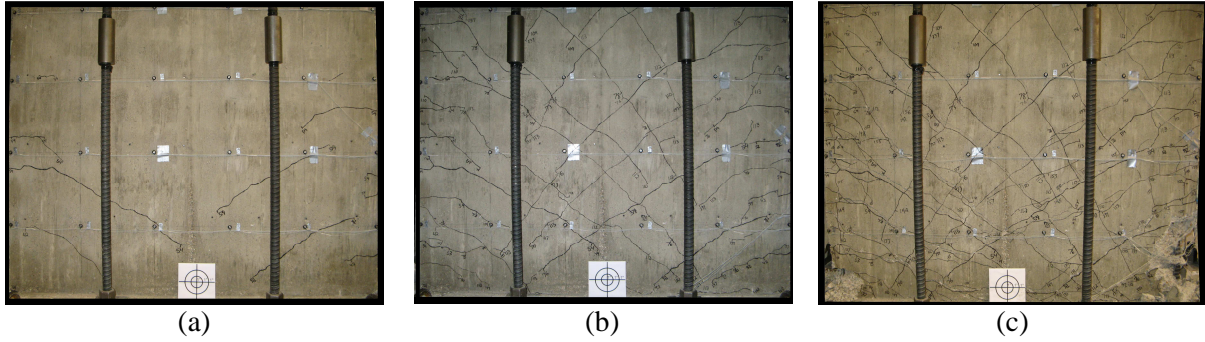


Figure 7: Crack patterns for limit states: (a) Flexural cracking. (b) First yield (c) Ultimate capacity

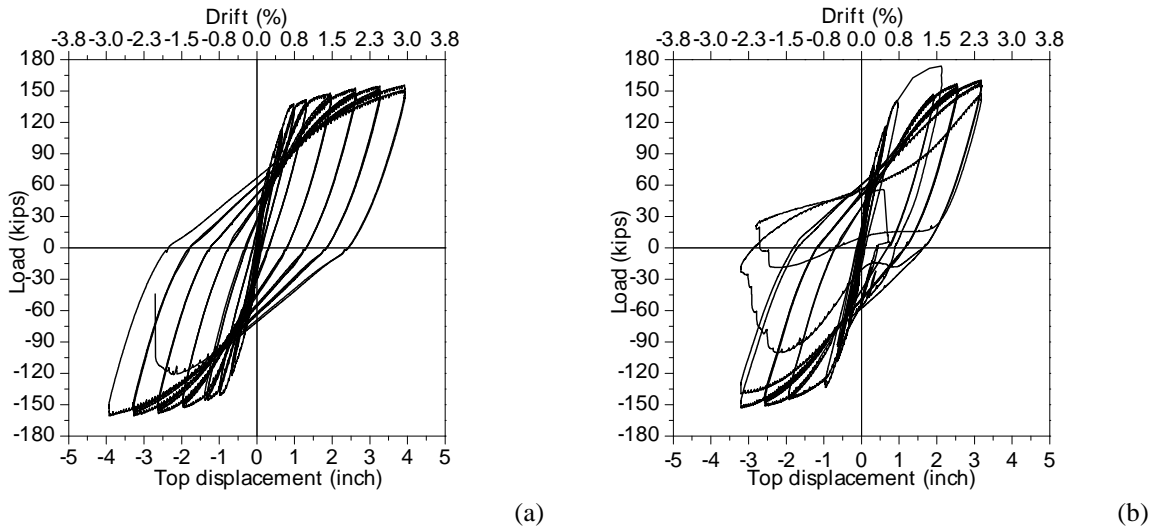


Figure 8: Load versus top displacement hysteresis curve (a) W-MC-C (b) W-MC-N

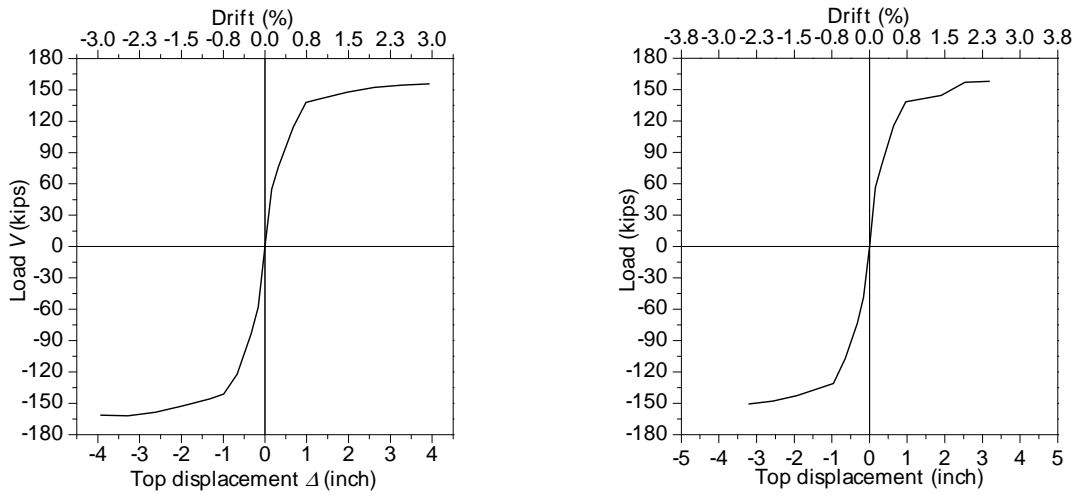
## 5. DISCUSSION OF TEST RESULTS.

### 5.1. Limit states.

Table 2 summarizes the values of displacement,  $\Delta$ , and force,  $V$ , for the following limit states proposed by Priestly et al. (2007) i) flexural cracking  $\Delta_{cr}$  and  $V_{cr}$  ii) First yield  $\Delta_y$  and  $V_y$  iii) Ultimate capacity  $\Delta_u$  and  $V_u$ . Comparing the results between specimens its worth noting that there was not a great difference in the response for the flexural cracking and first yield states. For the ultimate capacity state, although a similar ultimate lateral load was reached by both specimens, the one with confinement had a greater lateral deformation, hence a greater ductility as can be observed in Figure .

Table 2:  $\Delta$ - $V$ , Member limit states.

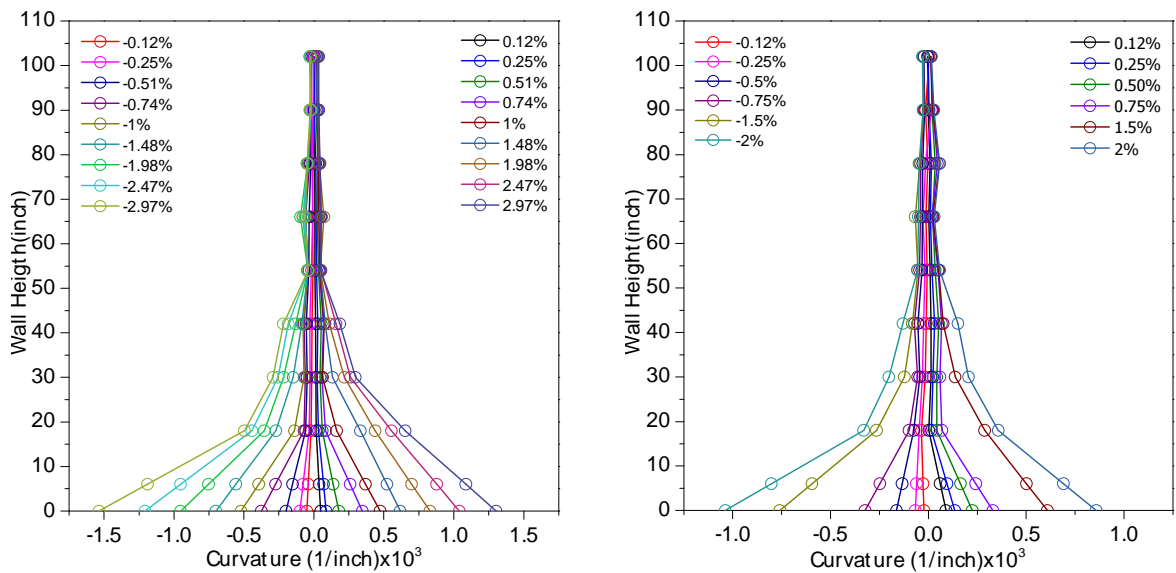
W-MC-C						W-MC-N					
$\Delta_{cr}$	$V_{cr}$	$\Delta_y$	$V_y$	$\Delta_u$	$V_u$	$\Delta_{cr}$	$V_{cr}$	$\Delta_y$	$V_y$	$\Delta_u$	$V_u$
(inch)	(inch)	(inch)	(kips)	(inch)	(kips)	(inch)	(kips)	(inch)	(kips)	(inch)	(kips)
0.16	58	0.98	141	3.93	161	0.16	56.3	0.96	138	3.18	157



(a) (b)  
 Figure 9: Load versus top displacement skeleton curve. (a) W-MC-C (b) W-MC-N

### 5.2. Curvature Distribution.

The maximum curvature for the different drift tests was obtained using the normal strains measured by the non-contact sensors grid overall the wall. Figure shows the distribution along the wall height of the mean values of the unit curvatures obtained for the 3 cycles at each drift level. As can be seen de maximum curvature observed at the same drift was almost equal for both specimens. The curvature profile seems to be approximately linear within a height equal to  $0.5h_w$ . Considering the plastic hinge length as the height above the foundation for which the curvature was equal to the yield curvature the results presented herein suggest that the plastic hinge length is approximately also  $0.5 h_w$ .



(a) (b)  
 Figure 10: Curvature distribution over the height at different drift sets. (a) W-MC-C (b) W-MC-N

### 5.3. Strain distribution.

Based on the measurements from a dense array of optical sensors the normal strains were determined along the wall height. Figure 2 show the strains measured in a 60inch x 60inch grid at the wall base for the 0.75% and 2% drift tests. As can be seen for the 0.75% drift test the unit tensile strains are greater

for the W-MC-C wall with maximum unit strain value of approximately  $\epsilon=12000 \mu\text{m/m}$  versus the  $\epsilon=9000 \mu\text{m/m}$  measured for the W-MC-N. On the other hand the maximum unit compressive strain was oppositely with values approximately of  $\epsilon=-4000 \mu\text{m/m}$  versus the  $\epsilon=6000 \mu\text{m/m}$  measured for the W-MC-N specimen. It is also worth noting that the depth of the neutral axis is greater for the W-MC-N specimen. In the case of the 2.0% drift test similar unit tensile strains with maximum values approximately of  $\epsilon=30000 \mu\text{m/m}$  were measured. Despite the fact that both similar ranged similar maximum tensile strains the specimen W-MC-C concentrated the inelastic strains in a region bellow  $0.5 h_w$  while in the W-MC-N were spread over that range.

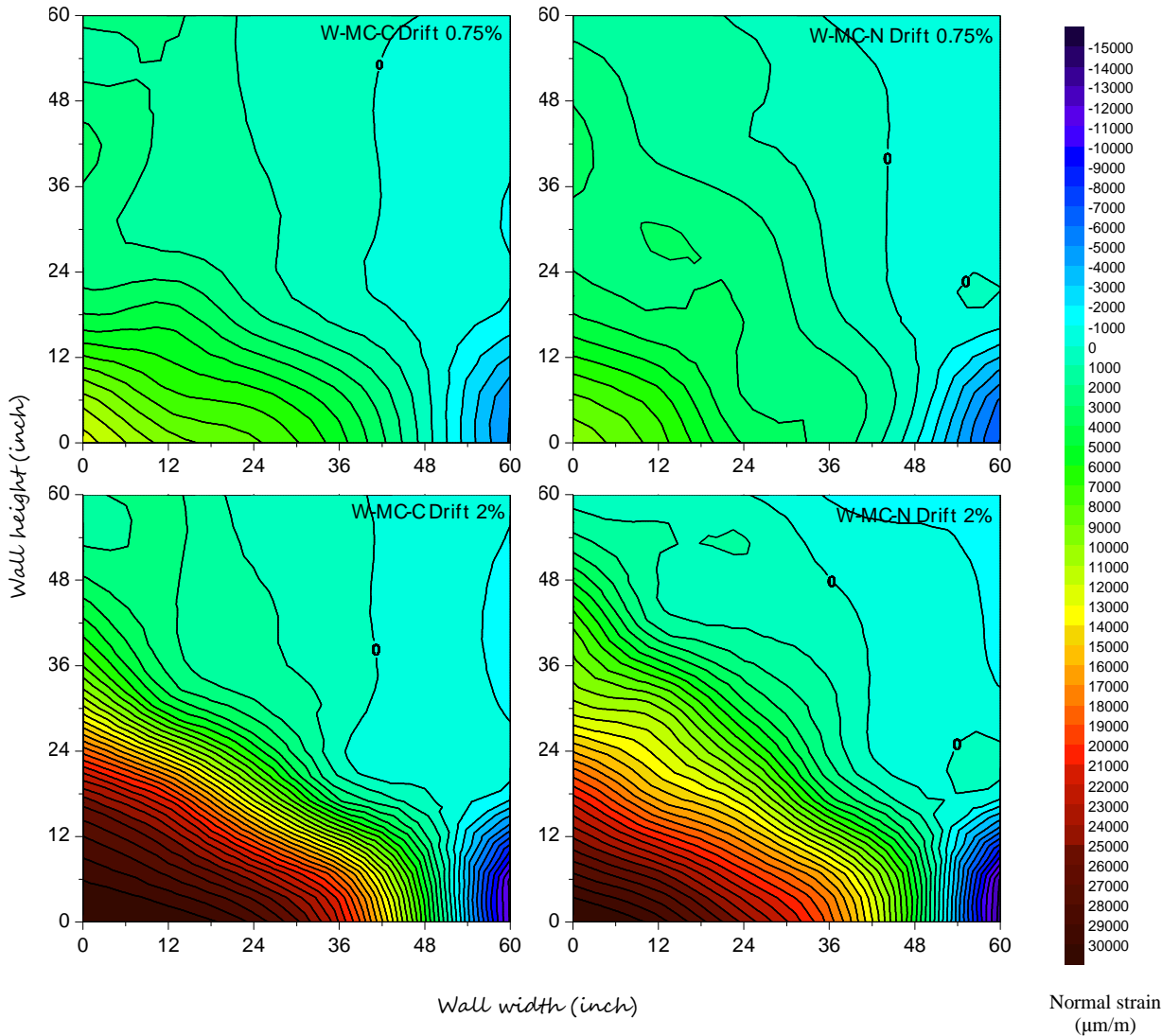


Figure 2: Strain distribution at the base at different drift sets.

**6. CONCLUSIONS.**

This paper presented the results of cyclic loading tests on two large-scale reinforced concrete structural walls conducted at Purdue University. One of the structural walls had confinement reinforcement meeting ACI-318-11 requirements while the other wall did not have any confinement reinforcement. The objective in this research was to investigate the effects of confinement on failure mode. The main findings of this experimental study may be summarized as follows:

- The confinement did not affect to the yielding force nor to the maximum lateral load.
- The inclusion of confinement reinforcement increased the maximum lateral displacement



capacity, hence the ductility and energy dissipation.

- The inelastic curvatures are concentrated at the wall base, approximately at a height of 0.5 times the wall depth.
- Specimen W-MC-C concentrated the inelastic strains in a region below  $0.5 h_w$  while in the W-MC-N were spread over that range.

## ACKNOWLEDGEMENT

Financial support from the Spanish Ministry of Science and Innovation, Project BIA2008/00050 and Fonds Européen de Développement Regional (FEDER) is acknowledged.

## REFERENCES

- ACI Committee 318 (2011). 318-11: Building Code Requirements for Structural Concrete and Commentary. American Concrete Institute.
- Bae, S. & Bayrak, O. (2008). Plastic hinge length of reinforced concrete columns. *ACI Structural Journal*, **105:3**, 290-30.
- Bohl, A., & Perry, A. (2011). Plastic hinge lengths in high-rise concrete shear walls. *ACI Structural Journal*, **108:2**, 148-157.
- Dazio, A., Beyer, K., & Bachmann, H. (2009). Quasi-static cyclic tests and plastic hinge analysis of RC structural walls. *Engineering Structures*. **31:7**, 1556-1571. doi:10.1016/j.engstruct.2009.02.018
- Hidalgo, P. A., Ledezma, C. A., & Jordan, R. M. (2002). Seismic Behavior of Squat Reinforced Concrete Shear Walls. *Earthquake Spectra*, **18:2**, 287. doi:10.1193/1.1490353
- Krolicki, J., Maffei, J., & Calvi, G. M. (2011). Shear Strength of Reinforced Concrete Walls Subjected to Cyclic Loading. *Journal of Earthquake Engineering*, 15(sup1), 30-71. doi:10.1080/13632469.2011.562049
- Pilakoutas, K., & Elnashai, A. (1995). Cyclic Behaviour of Reinforced Concrete Cantilever Walls, Part I: Experimental Results. *ACI Structural Journal*, **92:3**, 271-281.
- Pilakoutas, K., & Elnashai, A. S. (1995). Cyclic Behavior of Reinforced Concrete Cantilever Walls , Part II : Discussions and Theoretical Comparisons. *ACI Structural Journal*. **92:4**, 425-433.
- Priestly, M.J.N., Calvi, G.M. & Kowalsky, M.J. (2007). Displacement-Based Seismic Design of Structures. IUSS Press, Pavia, Italy.
- Priestly, M.J.N. & Paulay, T. (1992). Seismic Design of Reinforced Concrete and Masonry Buildings. John Wiley & sons, Inc.
- Priestly, M. J. N., & Park, R. (1987). Strength and Ductility of Concrete Bridge Columns Under Seismic Loading. *ACI Structural Journal*, **January-February**, 61-76.
- Sheikh, S. A., & Houry, S. S. (1993). Confined concrete columns with stubs. *ACI Structural Journal*, **90**, 414-414.